Available online at www.sciencedirect.com

ScienceDirect

Ceramics International 41 (2015) 1107–1114

CERAMICS INTERNATIONAL

www.elsevier.com/locate/ceramint

Experiments and numerical simulations of thermal shock crack patterns in thin circular ceramic specimens

Yuxing Liu[a], Xiaofeng Wu[b], Qiankun Guo[b], Chiping Jiang[b,c], Fan Song[c,*], Jia Li[d]

[a]School of Materials Science and Engineering, Beihang University, Beijing 100191, People's Republic of China
[b]School of Aeronautic Science and Engineering, Beihang University, Beijing 100191, People's Republic of China
[c]State Key Laboratory of Nonlinear Mechanics, Institute of Mechanics, Chinese Academy of Sciences, Beijing 100190, People's Republic of China
[d]LSPM, CNRS UPR 3407, Université Paris XIII, 99 Avenue Jean-Baptiste Clément, Villetaneuse 93430, France

Received 24 July 2014; received in revised form 6 September 2014; accepted 7 September 2014
Available online 16 September 2014

Abstract

An attempt was made to explore the formation mechanism of thermal shock crack patterns in ceramics and to develop quantitative numerical simulations. A set of experiments on thin circular ceramic specimens yielded two-dimensional readings of thermal shock crack patterns with periodical and hierarchical characteristics. The numerical simulations of the thermal shock crack patterns are based on the minimum potential energy principle, where the convective heat transfer coefficient at high temperatures, which is difficult to measure, was inversely estimated by the crack spacing, which is easy to measure. Numerical simulation results were in good agreement with the experimental data. Several interesting thermal shock crack evolution phenomena were found. Two stability criteria of crack propagation, i.e. the minimum potential energy principle and the fracture mechanics bifurcation theory, were compared. It was found that the two criteria verify and complement each other. The present study leads to an improved understanding of the formation and evolution of thermal shock crack patterns in ceramics and can help engineers to assess the thermal shock failure of practical ceramic components.

Keywords: Ceramics; Thermal shock; Crack patterns; Numerical simulations

1. Introduction

The chemical stability of ceramics above the melting point of metal alloys predestines this class of materials for high temperature applications such as gas turbine engines [1] for aircraft propulsion, marine propulsion, power generation and thermal protection structures in hypersonic vehicle [2,3]. However, thermal shock failure of ceramics is a long-standing problem [4]. It is recognized that a basic understanding of thermal shock failure must be gained to give full play to the potential of ceramic materials at high temperatures [1].

Numerous studies were conducted to explore the mechanism of thermal shock failure of ceramics. Among them, Kingery [5] and Hasselman [6] proposed two theories of thermal shock resistance from the viewpoint of stress and energy, respectively. Soon afterwards, Hasselman [7] developed a unified theory to combine thermal shock fracture initiation with crack propagation in brittle ceramics. Schneider [8] studied thermal shock parameters that depend on crack initiation and arrest criteria for ceramics, and discussed the role of thermal shock experiments. Salvini et al. [9] extended Hasselman's thermal shock theory [7] by considering the crack interaction mechanisms with the refractory microstructure.

Thermal shock resistance of ceramics is commonly evaluated by the degradation of the strength after thermal shock which is caused by the appearance of cracks. Researchers very early noticed that thermal shock cracks exhibit generally regular and elegant patterns, such as periodic and hierarchical characteristics, which are important for a clear understanding of the thermal shock failure mechanism of ceramics. Bažant [10] and Nemat-Nasser et al. [11,12] studied the stability of

*Corresponding author. Tel.: +86 10 8254 3961; fax: +86 10 8254 3935.
E-mail address: songfan.imech@gmail.com (F. Song).

http://dx.doi.org/10.1016/j.ceramint.2014.09.036
0272-8842/

propagated thermal shock cracks (or drying shrinkage cracks), and theoretically discussed the length hierarchy phenomenon. Bahr et al. [13–15] established a fracture-mechanical model based on the time-dependent energy release rate to explain the thermal shock cracking behaviors. Jenkins [16] used a method based on energy minimization to determine the spacing and penetration of a regular array of cracks in a shrinking slab due to a changing temperature field. Jiang et al. [17] conducted thermal shock experiments of thin rectangular ceramic specimens and developed numerical simulations of thermal shock crack patterns. Li et al. [18] proposed a non-local failure model to simulate the thermal shock crack evolution. Bourdin et al. [19] conducted numerical simulation of reservoir stimulation based on the variational approach. Furthermore, Bourdin et al. [20] and Sicsic et al. [21] studied the morphogenesis, initiation, and propagation of cracks in the thermal shock problem through the variational analysis of the quasi-static evolution of a gradient damage model.

The present work constitutes a continuing study on thermal shock crack patterns in ceramics and the emphasis is on an improved understanding of the formation and evolution mechanism as well as the development of quantitative numerical simulations of thermal shock crack patterns. To eliminate the boundary effects and to yield two-dimensional readings of crack patterns which are convenient to measure quantitatively, a set of thermal shock experiments on thin circular specimens were conducted. Then the crack patterns were numerically simulated based on the minimum potential energy principle. Finally, we made comparison of two stability criteria of crack propagation and comparison with experiments to reveal the evolution and bifurcation mechanism of thermal shock crack patterns.

2. Experimental

99% Al_2O_3 powder (University of Science and Technology Beijing Experimental Factory Co., Beijing, China) was thermoformed into thin circular plates with dimensions of 13 mm diameter and 1 mm thickness. Then the specimens were polished and tightly stacked together in sets of four, with two thick circular ceramic plates on the outside to prevent the temperature distribution from being disturbed by coolant accessing the interior surfaces of the specimens. For the convenient of binding, cross notches were carved on the outside surfaces of the two thick plates. Finally, the stacks of alumina circular specimens were bound with inconel wires, as shown in Fig. 1.

The bound specimens were heated in a furnace at a rate of 10 °C min^{-1} to the preset temperature T_0 and maintained at this temperature for 30 min. The range of T_0 was from 250 °C to 500 °C. The heated specimens were dropped into a water bath at $T_1 = 15$ °C by free fall. The specimens were removed from the water bath 10 min later and dried, then dyed with blue ink to observe the cracks formed. Two sets of specimens (8 specimens in total) were tested at every value of T_0.

The digitally scanned photographs of dyed specimens are shown in Fig. 2. It is observed that the thermal shock cracks are perpendicular to the circle edge and point to the center.

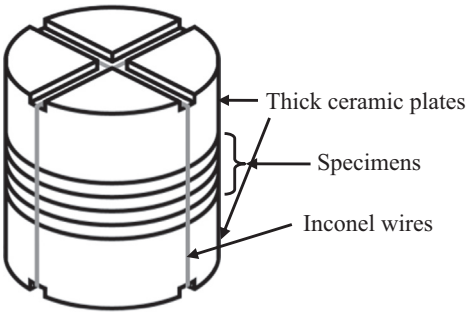

Fig. 1. Bound specimens for thermal shock.

In addition, the crack patterns on both sides of the specimen are identical, which shows that the crack geometry is two-dimensional and convenient to observe and measure. Furthermore, it is observed that the crack patterns exhibit elegant periodic and hierarchical characteristics that vary with the thermal shock temperature T_0. The higher the T_0, the more the cracks. The long cracks become longer and the short cracks become shorter as T_0 increases.

The variations in the average crack spacing $\bar{s}_0$ with the thermal shock temperature T_0 are depicted in Fig. 3, where the average crack spacing $\bar{s}_0$ means the arc length on the outer circular circumference between two adjacent cracks. It can be seen that at every value of T_0, the fluctuation in the average crack spacing, $\bar{s}_0$, in eight specimens is small, and the maximum standard deviation from the average value is less than 15%. At the same time the crack spacing $\bar{s}_0$ decreases with the increase of T_0.

In the following sections an attempt is made to quantitatively simulate thermal shock crack patterns as well as to reveal the mechanism of formation and evolution of thermal shock crack patterns, especially the interesting bifurcation mechanism.

3. Numerical simulations

In the study of thermal shock crack patterns, two main approaches are the fracture mechanics bifurcation theory and the energy minimization method. In this section, numerical simulations based on the minimum potential energy principle will be developed. Then in the next section, comparisons will be made with results of fracture mechanics bifurcation theory and experimental data.

3.1. Assumptions

According to the experimental observations, three simplified assumptions are made: (1) The cracks are two-dimensional, and perpendicular to the outer circular circumference of specimens. (2) The crack patterns are periodic and hierarchical, consequently they can be simulated by a periodic unit. (3) From the assumption (1), the temperature field is not disturbed by the cracks, consequently it remains axisymmetric and is easily calculated by Fourier's law of heat conduction.

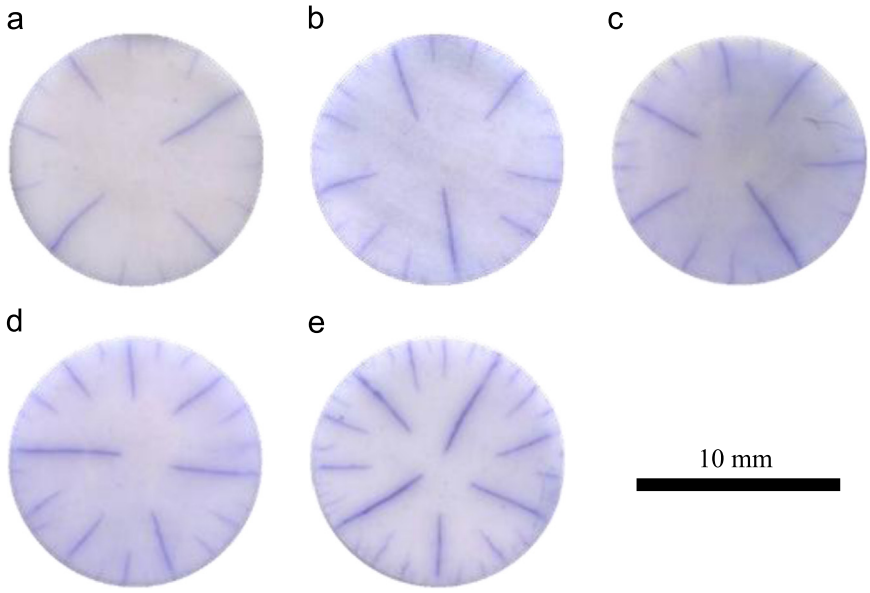

Fig. 2. Thermal shock crack patterns, where the preset temperature T_0=(a) 250 °C, (b) 300 °C, (c) 350 °C, (d) 400 °C, and (e) 500 °C.

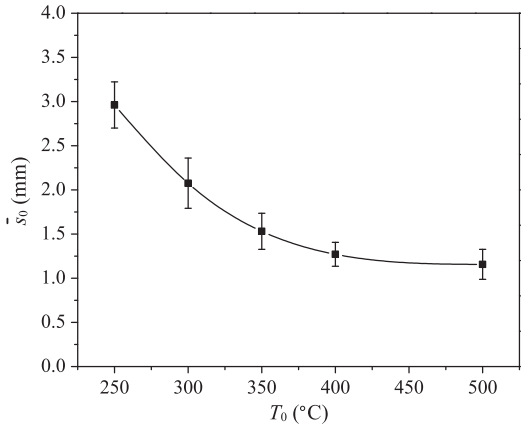

Fig. 3. Variations in the average crack spacing $\bar{s}_0$ (the arc length on the outer circular circumference between two adjacent cracks) in eight specimens with the thermal shock temperature T_0.

3.2. Theoretical considerations

The average total potential energy $\overline{W}$ in a specimen can be expressed as a function of the crack spacing s (the arc length on the outer circular circumference between two adjacent cracks), the crack length p, and the time t

$$\overline{W}(s,p,t)=\frac{W(s,p,t)}{V}=\frac{U(s,p,t)+S}{V}=\frac{U(s,p,t)+\gamma pb}{V} \quad (1)$$

where V is the volume of the specimen, U is the strain energy, $S=\gamma pb$ is the crack surface energy (the energy required to form new crack surfaces) and γ is the surface energy density, and b is the thickness of specimens.

According to the minimum potential energy principle, an optimal thermal shock crack pattern minimizes the average total potential energy

$$\overline{W}(s_0,p_0,t)=\min \overline{W}(s,p,t) \quad (2)$$

where p_0 and s_0 are the optimal crack length and spacing at the time t. Computations show that when the preset temperature T_0 is less than certain critical value T_c or the thermal shock time t is less than a certain critical value t_c, the minimum value on the curved surface of $\overline{W}$ is located at $p_0=0$, which indicates that the specimen does not crack. When $T_0>T_c$ and $t>t_c$, the minimum value of $\overline{W}$ shifts to a location where both s_0 and p_0 become positive finite values, which indicates that cracks initiate. An illustrative example is shown in Fig. 4, where $T_0=400$ °C, $t=0.002$ s and 0.008 s. Theoretically, the optimal thermal shock crack spacing and length (s_0, p_0) (the minimum value of the energy curved surface in Fig. 4) change continuously with time t. Computations show that in thermal shock process, the idealized crack length continuously increases from zero, whereas the crack spacing starts from a finite value, rapidly decreases and reaches its minimum value in a very short time, then increases.

However, the irreversibility of crack growth prohibits the continuous change of crack spacing with time. Therefore, the minimum energy principle should be a conditional minimum potential energy principle. The condition is that the formed cracks do not move, recede or disappear. Our computations show that when the cracks initiate, their spacing is a large finite value. The crack spacing first decreases by a jumping manner due to the appearance of additional cracks, then increases also by a jumping manner of "spatial period doubling", i.e. every second crack continues to propagate, whereas the other cracks stop. The process of "spatial period doubling" can be repeated, thus an elegant hierarchical thermal shock crack pattern is formed.

3.3. Semi-inverse method

The lack of accurate data of material properties at high temperatures is a challenge in quantitatively simulating thermal shock crack patterns. The available data [22–27] on the heat transfer coefficient

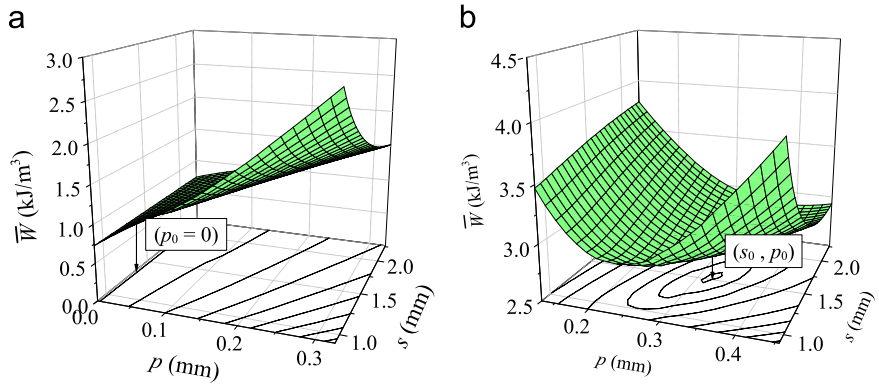

Fig. 4. Graphs of the average total potential energy curved surfaces at T_0=400 °C for two time points, (a) t=0.002 s; (b) t=0.008 s.

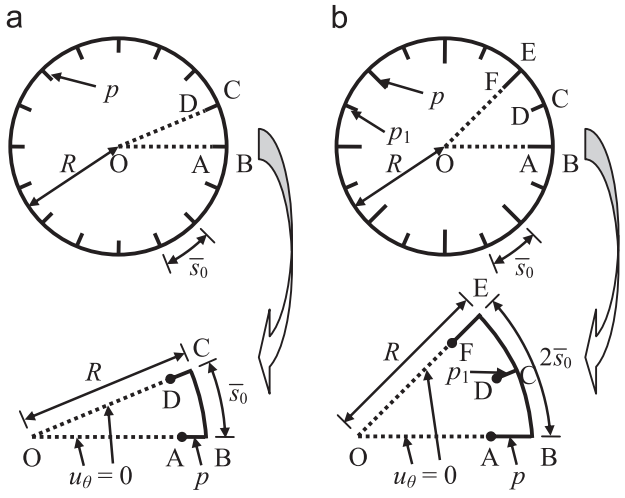

Fig. 5. Computational region and boundary conditions: (a) initial region, (b) extended region, where p and p_1 represent the length of propagating and stationary cracks, respectively, and dotted lines represent the uncracked boundaries.

h for water quenching of ceramics are very disperse, with a consensus being between 10^4 and 10^5 W/(m^2 K). Apparently, such dispersion prohibits any quantitative simulation of thermal shock crack patterns. From our experiments (for example, refer to Fig. 3), we find that crack spacing is easily measured from experiments and the standard deviation from the average crack spacing is small. In addition, our computations show that the idealized crack spacing reaches its minimum value in a very short time. Accordingly, we presented a semi-inverse method [17] combining experimental and numerical analysis, where effective convective heat transfer coefficients $\overline{h}$ are inversely estimated using the experimental data of crack spacing which equal the minimum value of the idealized crack spacing. The semi-inverse method permits us to study the evolution of thermal shock crack patterns and to predict quantitatively crack length and length hierarchy. Furthermore, it is also an exploration to estimate a physical quantity difficult to measure by using physical quantities easy to measure.

3.4. Computational region and material properties

The finite element software ANSYS was used for the numerical simulations. Noting the axisymmetry, a sector OABCD in Fig. 5(a) was taken as the initial computational region, where R is the radius of the specimen, A and D are the crack tips. Noting that the central angle of the sector remains unchanged, the circumferential displacement u_θ is zero on two radius boundaries

$$u_\theta = 0, \text{ on OA and OD} \tag{3}$$

The other boundaries are traction-free.

When "spatial period doubling" of the crack spacing appears, the computational region would be extended to the sector OABCEF in Fig. 5(b), where D is a stationary crack tip, A and F are two propagating crack tips. Such an extension of the computational region can be repeated.

According to our experience, the computational time t was taken as 1 s, which was divided into 500 time steps, and the step length of the crack length p was taken as R/100.

Young's modulus E [28], Poisson's ratio ν [28], the mass density ρ [28], and the surface energy density γ [29] of the material remain approximately unchanged in the range 0–600 °C, which are listed in Table 1. The coefficient of thermal expansion α [30], the thermal conductivity k [31] and the specific heat c [32] are strongly temperature-dependent, which are shown in Fig. 6.

Table 1
Young's modulus E [28], Poisson's ratio ν [28], the mass density ρ [28], and the surface energy density γ [29] of 99% Al_2O_3 ceramics.

E (GPa)	ν	ρ (kg/m^3)	γ (J/m^2)
370	0.22	3980	12.16

Based on the "semi-inverse method" and using the data of the crack spacing depicted in Fig. 3, the estimated values of the effective convective heat transfer coefficient $\overline{h}$ at various values of T_0 are shown in Fig. 7. It can be observed that $\overline{h}$ first rapidly increases, then decreases, with a peak near T_0=350 °C.

It is interesting to compare the present estimates of the convective heat transfer coefficient with existing data: (1) because of the difficulties of measurement, no direct measurement data were reported. Existing data of the coefficient were estimated by measuring the critical temperature differences according to the theory of critical fracture stress [22–24] or by solving the inverse heat conduction problem based on the

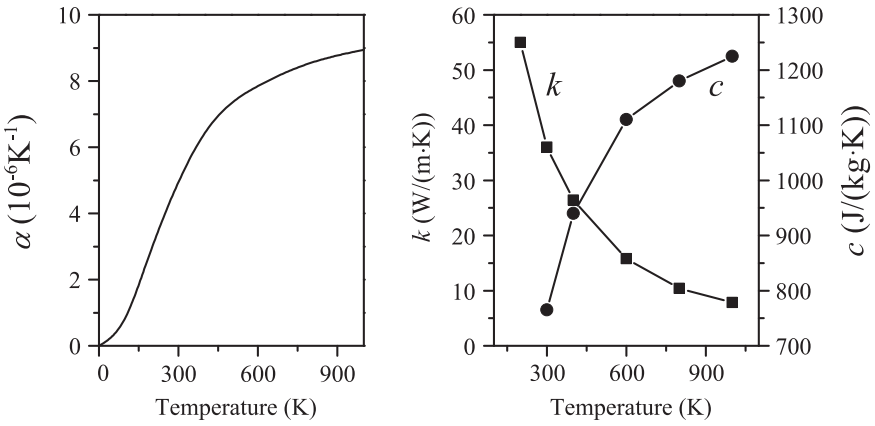

Fig. 6. Graphs of the coefficient of thermal expansion α [30], the thermal conductivity k [31], and the specific heat c [32] of 99% Al_2O_3 ceramics versus temperature.

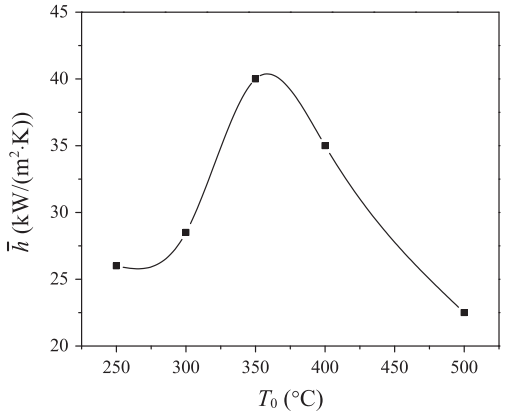

Fig. 7. Effective heat transfer coefficient $\overline{h}$ estimated by semi-inverse method at various values of T_0.

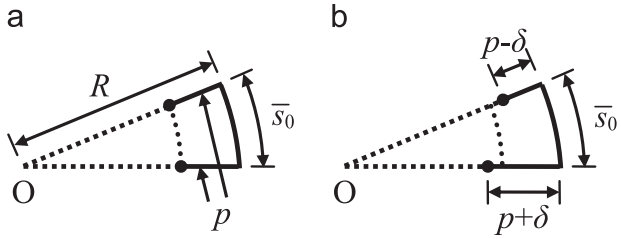

Fig. 8. Crack propagation models: (a) equal-length crack model and (b) corresponding disturbed crack model, where the disturbance quantity $\delta = R/200$.

measurement of the temperature distribution in the specimens during thermal shock [25–27]. The present semi-inverse method is a new exploration where the coefficient is estimated by using the crack spacing. (2) The variation law of the coefficient with temperature estimated by using the present semi-inverse method is in agreement with that of existing data, i.e., the coefficient first increases to a peak value, then decreases (refer to Fig. 7). (3) Because the estimation of the coefficient involves a number of parameters including environmental variables, material properties, and geometry effects, the dispersion of existing data is very large. For example, the peak values of the coefficient are 100,000 W/(m^2 K) in [22,23], 45,000 W/(m^2 K) in [24], 63,000 W/(m^2 K) in [25,26], and 29,300 W/(m^2 K) in [27]. The present estimated peak value, 40,000 W/(m^2 K), of the coefficient falls within the scope of variation of existing data. (4) The present estimates of the coefficient can be used to quantitatively predict the length and length hierarchy of thermal shock cracks in the present experiment (refer to Fig. 11), while existing data failed to do this.

3.5. Stability criteria of crack propagation

From Section 3.2, in a very short time the thermal shock crack spacing reaches its minimum value and the experimental data of the average crack spacing are used to estimate inversely the effective heat transfer coefficients $\overline{h}$. Then the crack spacing increases by a jumping manner of "spatial period doubling", i.e. every second crack continues to propagate, whereas the other cracks stop. Consequently a hierarchical crack pattern is formed. Therefore, a key work in numerical simulations is to build a stability criterion of crack propagation, which determines when "spatial period doubling" of the crack spacing occurs.

Referring to Fig. 8(a), at every time step, first consider the equal-length crack model. The crack length p can be determined by the minimum potential energy principle. Let W_e denote the corresponding minimum energy of the equal-length crack model. Then we consider a disturbed crack model, as shown in Fig. 8(b), where the disturbance $\delta = R/200$ (from our experience), R is the radius of the circular specimen. Let W_d denote the corresponding energy of the disturbed model. Consider the difference of the two energy

$$\Delta W = W_d - W_e \tag{4}$$

Apparently, if $\Delta W > 0$, the equal-length model is stable; whereas if $\Delta W \le 0$, the equal-length model is unstable. In the latter case, "spatial period doubling" of the crack spacing appears. Such a process of "spatial period doubling" of the crack spacing can be repeated to form a hierarchical crack patterns.

3.6. Numerical simulation results

The numerical simulations developed in the above sections can reproduce the evolution process of thermal shock crack

patterns (length and length hierarchy), which is difficult to observe and measure in experiments.

As an illustrative numerical example, the evolutions of the crack spacing s and crack length p with time t at $T_0=400$ °C are plotted in Fig. 9, where the solid line and the dashed line represent the spacing and the length of the propagating cracks, respectively.

It can be observed from the inset of Fig. 9 that in a very short time, the thermal shock cracks initiate and the idealized crack spacing denoted by the dot dashed line rapidly reaches its minimum value (at $t=0.01$ s). The stage is very short and the variation of the practical crack spacing is difficult to predict. Apparently, it is a good alternative scheme that the practical crack spacing is taken from experimental data, which are easy to measure.

Fig. 9 shows that after the thermal shock cracks initiate, the cracks propagate very rapidly, then the propagation speed decreases gradually with the release of thermal stress until the strain energy cannot support the simultaneous propagation of all cracks. At this time "spatial period doubling" of the crack spacing appears, i.e. every second crack continues to propagate with an equal spacing $s=2\bar{s}_0$, whereas the other cracks stop. After "spatial period doubling" of the crack spacing appears, the crack propagation speed shows a sudden increase as the strain energy supports propagation of only half of the cracks. This process can be repeated until the strain energy induced by thermal stress cannot support the propagation of any cracks.

4. Comparison and discussion

4.1. Comparison of two stability criteria of crack propagation

In the study of thermal shock crack patterns, a widely used method is the fracture mechanics bifurcation theory, for example refer to [33–35]. The theory uses the stability criterion of crack propagation based on the stress intensity factor or the energy release rate. First we consider the equal-length crack model in Fig. 8(a). From mechanical equilibrium, we have

$$K_I = K_{IC} \tag{5}$$

where K_I and K_{IC} are the stress intensity factor at the crack tip and the fracture toughness of the material, respectively. Then we consider the disturbed crack model, as shown in Fig. 8(b), where the disturbance $\delta=R/200$ in our computations. Let K_{Il} and K_{Is} be the stress intensity factors at long and short crack tips, respectively. If

$$K_{Il} < K_{IC}, K_{Is} > K_{IC} \tag{6}$$

the long crack in Fig. 8(b) will stop growing, whereas the short crack will grow and catch up with the long crack, which shows that the equal-length crack model is stable. If

$$K_{Il} \geq K_{IC}, K_{Is} \leq K_{IC} \tag{7}$$

the short crack in Fig. 8(b) will stop growing, whereas the long crack will continue to grow, which shows that the equal-length crack model is unstable and hierarchy of crack length occurs. Noting that the equal-length crack model satisfies the condition (5), the stability criterion of crack propagation can be expressed by

$$\Delta K = K_{Is} - K_{Il} \tag{8}$$

When $\Delta K \geq 0$, the equal-length crack model is stable, whereas when $\Delta K < 0$, the equal-length crack model is unstable and hierarchy of crack length occurs.

The stress intensity factor is a local mechanical quantity at the crack tip, whereas the total potential energy is a whole mechanical quantity of the specimen. It is interesting to compare the two stability criteria of crack propagation by using ΔW in Eq. (4) and ΔK in Eq. (8).

The variations of ΔW and ΔK with the crack length p at $T_0=400$ °C before and after first crack length hierarchy are shown in Fig. 10. It can be observed that when p is a small value, both ΔK and ΔW are positive, which indicates that equal-length crack propagation is stable. Both ΔK and ΔW decrease with the increase of p, which indicates that equal-length crack propagation gradually changes from stability to instability. Both ΔK and ΔW change signs almost at the same length $p=0.72$ mm, which indicates that equal-length crack propagation becomes unstable, consequently "spatial period doubling" of the crack spacing occurs, i.e. every second crack continues to propagate, whereas the other cracks stop. After "spatial period doubling" of the crack spacing occurs, both ΔK and ΔW jump to large value, which indicates that such a propagation of cracks is highly stable. Then both ΔK and ΔW decrease with the increase of p and change again their signs at $p=1.76$ mm, which indicates second "spatial period doubling" of the crack spacing occurs. The process can be repeated and forms a hierarchical crack pattern. Fig. 10 shows the equivalence of two stability criteria of crack propagation. Such finding improves our understanding of the formation mechanism of thermal shock crack patterns.

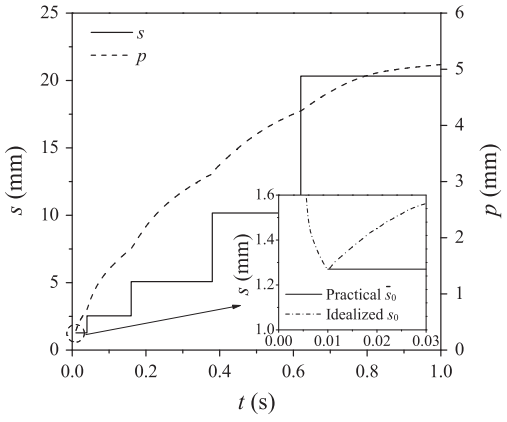

Fig. 9. Evolution of the crack spacing s and crack length p with time t at $T_0=400$ °C, where the solid and dashed lines represent the spacing s and the length p of the propagating cracks, respectively. In the inset the dot dash line denotes the idealized crack spacing s_0, and the solid line denotes the practical average crack spacing $\bar{s}_0$ taken from the experimental datum in Fig. 3.

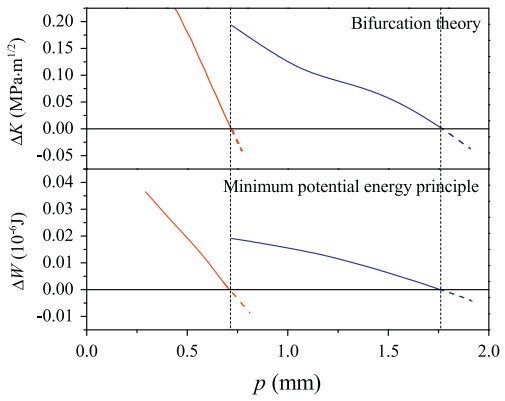

Fig. 10. Variations of ΔW and ΔK with crack length p at $T_0=400$ °C before and after first crack length hierarchy.

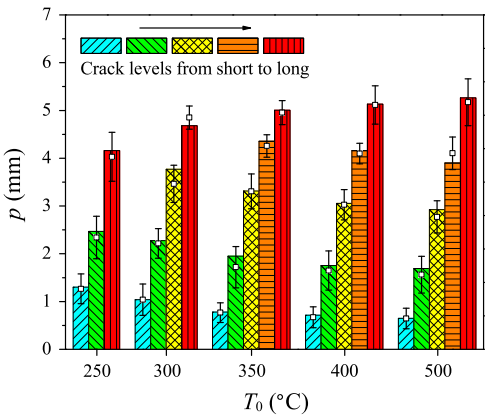

Fig. 11. Numerical predictions of various level crack lengths p versus the preset temperature T_0, the corresponding classified experimental results are also shown by points with error bar.

4.2. Comparison with experiments

It can be seen from Figs. 2 and 3 that the experimental data of thermal shock crack patterns exhibit some degree of dispersion. Numerical simulations can help us find the essential feature from uncertainty. Now consider the hierarchy of the crack length. According to the hierarchical mechanism described in Section 3.5, the ratio of the crack number of various levels for a three-level crack pattern is 2:1:1 from short to long, it is 4:2:1:1 for a four-level crack pattern and 8:4:2:1:1 for a five-level crack pattern. According to the above ratios, the experimental statistical results of the thermal shock crack length were classified and depicted in Fig. 11 by points with error bar. Additionally, the numerical simulation results of the various level crack lengths p versus the preset temperature T_0 are also shown in Fig. 11 by column chart. It can be seen that the numerical predictions are in good agreement with experimental results.

It is also observed that the crack length of every level continuously changes with the increase of preset temperature T_0. An interesting phenomenon is found: the crack length of the longest level increases with the increase of T_0, whereas the crack lengths of the other levels decrease. When ΔW in Eq. (4) (or ΔK in Eq. (8)) goes across zero, a new crack level is separated from the longest crack level. Then the length of the new crack level decreases with the increase of T_0.

4.3. Discussion about the crack spacing in the computational model

In the present computational model the assumptions of a circular geometry and regular spacing require that the crack spacing s can take on discrete values only, i.e.

$$s = R \times 2\pi/n, \quad \text{for } n = 1, 2, 3, \ldots \tag{9}$$

where n is the crack number and R is the radius of the specimen. In the practical numerical simulations, however, the crack spacing s of the computational unit is taken from the average value $\bar{s}_0$ of experimental data among eight specimens, where corresponding n is not an integer. By comparing $\bar{s}_0$ with the crack spacing s that is corresponding to an integer value of n and is closest to $\bar{s}_0$, we found that the maximum deviation between $\bar{s}_0$ and s is less than 1.7% which is small enough and can be ignored.

5. Conclusions

(1) A set of water-quenching experiments on thin circular ceramic specimens at various preset temperatures yielded elegant two-dimensional thermal shock crack patterns. It is observed that the crack patterns exhibit favorable periodic and hierarchical characteristics that vary with the thermal shock temperature. The higher the temperature, the more the cracks. In addition, the long cracks become longer and the short cracks become shorter as T_0 increases. At the same thermal shock temperature the dispersion in the number of cracks (or the average crack spacing) in various specimens is small.

(2) Based on the minimum potential energy principle, numerical simulations were developed to investigate the evolution of crack patterns during the thermal shock process. To overcome the difficulty in measuring accurately the convective heat coefficient at high temperatures, a so-called "semi-inverse method" was developed, where the effective convective heat coefficient was inversely estimated by using the experimental data of crack spacing which is easy to measure. The "semi-inverse method" explores a new approach of practical importance, i.e. to estimate a physical quantity difficult to measure by using physical quantities easy to measure. The numerical predictions of the crack length and length hierarchy are in good agreement with experimental results.

(3) Two stability criteria of crack propagation, i.e. the minimum potential energy principle and the fracture mechanics bifurcation theory, were compared. The former is based on a whole physical quantity, the total potential energy of the specimen, whereas the latter is based on a local physical quantity, the stress intensity factor at the crack tip. It is found that the simulations by the two criteria are in excellent agreement. The two criteria verify and complement each other.

(4) Numerical simulations can conveniently reproduce the evolution process of thermal shock crack patterns, which

is difficult to observe by experiments. It is found that the crack length of every level continuously changes with the increase of preset temperature T_0. The crack length of the longest level increases with the increase of T_0, whereas the crack lengths of the other levels decrease. New crack levels are always separated from the longest crack level. Then the length of the new crack level decreases with the increase of T_0. The present study leads to an improved understanding of the formation and evolution of thermal shock crack patterns in ceramics.

Acknowledgments

This work was supported by the National Natural Science Foundation of China (Grants nos. 11172023 and 11232013), the Fundamental Research Funds for the Central Universities and funding from the French ANR program T-Shock ANR-10-INTB-0915.

References

[1] N.P. Padture, M. Gell, E.H. Jordan, Thermal barrier coatings for gas-turbine engine applications, Science 296 (2002) 280–284.
[2] S.R. Levine, E.J. Opila, M.C. Halbig, et al., Evaluation of ultra-high temperature ceramics for aeropropulsion use, J. Eur. Ceram. Soc. 22 (14,15) (2002) 2757–2767.
[3] M.M. Opeka, I.G. Talmy, J.A. Zaykoski, Oxidation-based materials selection for 2000 °C hypersonic aerosurfaces: theoretical consideration and historical experience, J. Mater. Sci. 39 (2) (2004) 5887–5904.
[4] R. Danzer, et al., Fracture of ceramics, Adv. Eng. Mater. 10 (4) (2008) 275–298.
[5] W.D. Kingery, Factors affecting thermal stress resistance of ceramic materials, J. Am. Ceram. Soc. 38 (1) (1955) 3–15.
[6] D.P.H. Hasselman, Elastic energy at fracture and surface energy as design criteria for thermal shock, J. Am. Ceram. Soc. 46 (11) (1963) 535–540.
[7] D.P.H. Hasselman, Unified theory of thermal shock fracture initiation and crack propagation in brittle ceramics, J. Am. Ceram. Soc. 52 (11) (1969) 600–604.
[8] G.A. Schneider, Thermal shock criteria for ceramics, Ceram. Int. 17 (6) (1991) 325–333.
[9] V.R. Salvini, V.C. Pandolfelli, R.C. Bradt, Extension of Hasselman's thermal shock theory for crack/microstructure interactions in refractories, Ceram. Int. 38 (7) (2012) 5369–5375.
[10] Z.P. Bažant, H. Ohtsubo, K. Aoh, Stability and post-critical growth of a system of cooling or shrinkage cracks, Int. J. Fract. 15 (5) (1979) 443–456.
[11] S. Nemat-Nasser, Stability of a system of interacting cracks, J. Int. Eng. Sci. 16 (4) (1978) 277–285.
[12] S. Nemat-Nasser, L.M. Keer, K.S. Parihar, Unstable growth of thermally induced interacting cracks in brittle solids, Int. J. Solids Struct. 14 (6) (1978) 409–430.
[13] H.A. Bahr, G. Fischer, H.J. Weiss, Thermal-shock crack patterns explained by single and multiple crack propagation, J. Mater. Sci. 21 (8) (1986) 2716–2720.
[14] H.A. Bahr, H. Balke, M. Kuna, H. Liesk, Fracture analysis of a single edge cracked strip under thermal shock, Theor. Appl. Fract. Mech. 8 (1) (1987) 33–39.
[15] H.A. Bahr, H.J. Weiss, H.G. Maschke, F. Meissner, Multiple crack propagation in a strip caused by thermal shock, Theor. Appl. Fract. Mech. 10 (3) (1988) 219–226.
[16] D.R. Jenkins, Optimal spacing and penetration of cracks in a shrinking slab, Phys. Rev. E 71 (5) (2005) 056117.
[17] C.P. Jiang, X.F. Wu, J. Li, F. Song, Y.F. Shao, X.H. Xu, et al., A study of the mechanism of formation and numerical simulations of crack patterns in ceramics subjected to thermal shock, Acta Mater. 60 (11) (2012) 4540–4550.
[18] J. Li, F. Song, C.P. Jiang, Direct numerical simulations on crack formation in ceramic materials under thermal shock by using a non-local fracture model, J. Eur. Ceram. Soc. 33 (13–14) (2013) 2677–2687.
[19] B. Bourdin, C. Maurini, M. Knepley, Numerical simulation of reservoir stimulation – a variational approach, in: Proceedings of the Thirty-Sixth Workshop on Geothermal Reservoir Engineering, Stanford University, Stanford, California, 2011.
[20] B. Bourdin, J.J. Marigo, C. Maurini, P. Sicsic, Morphogenesis and propagation of complex cracks induced by thermal shocks, Phys. Rev. Lett. 112 (2014) 014301.
[21] P. Sicsic, J.J. Marigo, C. Maurini, Initiation of a periodic array of cracks in the thermal shock problem: a gradient damage modeling, J. Mech. Phys. Solids 63 (2) (2014) 256–284.
[22] P.F. Becher, D. Lewis III., K.R. Carman, A.C. Gonzalez, Thermal shock resistance of ceramics: size and geometry effects in quench tests, J. Am. Ceram. Soc. 59 (5) (1980) 542–545.
[23] P.F. Becher, Effect of water bath temperature on the thermal shock of Al_2O_3, J. Am. Ceram. Soc. 64 (1) (1981) C17–C18.
[24] J.P. Singh, Y. Tree, D.P.H. Hasselman, Effect of bath and specimen temperature on the thermal stress resistance of brittle ceramics subjected to thermal quenching, J. Mater. Sci. 16 (8) (1981) 2109–2118.
[25] Y. Kim, W.J. Lee, E.D. Case, The measurement of the surface heat transfer coefficient for ceramics quenched into a water bath, Mater. Sci. Eng. A 145 (1) (1991) L7–L11.
[26] W.J. Lee, Y. Kim, E.D. Case, The effect of quenching media on the heat transfer coefficient of polycrystalline alumina, J. Mater. Sci. 28 (8) (1993) 2079–2083.
[27] Z.L. Zhou, F. Song, Y.F. Shao, S.H. Meng, C.P. Jiang, J. Li, Characteristics of the surface heat transfer coefficient for Al_2O_3 ceramic in water quench, J. Eur. Ceram. Soc. 32 (12) (2012) 3029–3034.
[28] Y.L. Zhang, J.P. Ma, Applicable Ceramic Material Manual, Chemical Industry Press, Beijing, 2006 (in Chinese).
[29] Q.C. Zhang, Mechanical Properties of Ceramics, Science Press, Beijing, 1987 (in Chinese).
[30] D.L. Jiang, L.T. Li, S.X. Ouyang, J.L. Shi, China Materials Engineering Canon, Chemical Industry Press, Beijing, 2006 (in Chinese).
[31] Y.S. Touloukian, C.Y. Ho, Thermophysical properties of matter, Thermal Conductivity of Nonmetallic Solids, 2, Plenum Press, New York, 1972.
[32] Y.S. Touloukian, C.Y. Ho, Thermophysical properties of matter, Specific Heat of Nonmetallic Solids, 5, Plenum Press, New York, 1972.
[33] T. Boeck, H.A. Bahr, S. Lampenscherf, U. Bahr, Self-driven propagation of crack arrays: a stationary two-dimensional model, Phys. Rev. E 59 (2) (1999) 1408–1415.
[34] S. Nemat-Nasser, Y. Sumi, L.M. Keer, Unstable growth of tension cracks in brittle solids: stable and unstable bifurcations, snap-through, and imperfection sensitivity, Int. J. Solids Struct. 16 (11) (1980) 1017–1035.
[35] H.A. Bahr, H.J. Weiss, U. Bahr, M. Hofmann, G. Fischer, S. Lampenscherf, et al., Scaling behavior of thermal shock crack patterns and tunneling cracks driven by cooling or drying, J. Mech. Phys. Solids 58 (9) (2010) 1411–1421.